

Dual character of magnetism in EuFe_2As_2 : Optical spectroscopic and density-functional calculation study

S. J. Moon,¹ J. H. Shin,¹ D. Parker,^{2,*} W. S. Choi,¹ I. I. Mazin,² Y. S. Lee,³ J. Y. Kim,⁴ N. H. Sung,⁴ B. K. Cho,⁴ S. H. Khim,⁵ J. S. Kim,⁶ K. H. Kim,⁵ and T. W. Noh^{1,†}

¹*ReCOE & FPRD, Department of Physics and Astronomy, Seoul National University, Seoul 151-747, Korea*

²*Naval Research Laboratory, 4555 Overlook Avenue SW, Washington, DC 20375, USA*

³*Department of Physics, Soongsil University, Seoul 156-743, Korea*

⁴*Department of Nanobio Materials and Electronics and Department of Materials Science and Engineering, GIST, Gwangju 50-712, Korea*

⁵*CSCMR & FPRD, Department of Physics and Astronomy, Seoul National University, Seoul 151-747, Korea*

⁶*Department of Physics, POSTECH, Pohang 790-784, Korea*

(Received 13 April 2010; published 19 May 2010)

We investigate the electronic structure of EuFe_2As_2 using optical spectroscopy and density-functional calculations. At low temperature we observe the evolution of *two* gaplike features, one having a weak-coupling mean-field behavior and another with strongly nonmean-field behavior. Using band-structure calculations, we identify the former with a spin-Peierls-type partial gap in d_{yz} bands and the latter with the transition across the large exchange gap in d_{xz}/d_{xy} bands. Our results demonstrate that the antiferromagnetism in the ferropnictides is neither fully local nor fully itinerant but contains elements of both.

DOI: [10.1103/PhysRevB.81.205114](https://doi.org/10.1103/PhysRevB.81.205114)

PACS number(s): 74.25.Gz, 74.25.Jb, 75.30.Fv

The discovery of high-temperature superconductivity in the ferropnictides has stimulated great interest in investigating their physical properties.¹ As in the cuprates, the superconducting state of the ferropnictides is located in the vicinity of a magnetically ordered state. The parent ferropnictide compounds exhibit stripe-type antiferromagnetic (AFM) spin-density-wave (SDW) order²⁻⁵ while suppressing the AFM order by various means gives rise to the superconductivity.^{1,6-9} It is generally believed that the proximity to magnetism plays a crucial role in establishing electronic pairing.¹⁰

Numerous efforts have been made to elucidate the electronic-structure changes across the SDW transition of the ternary ferropnictide AFe_2As_2 ($\text{A}=\text{Ba}$, Sr , or Eu) compounds. In angle-resolved photoemission spectroscopy (ARPES) studies on BaFe_2As_2 and SrFe_2As_2 , the electronic-structure changes across the SDW transition were initially explained in terms of the exchange splitting,^{11,12} even though no uniform exchange splitting is expected in an antiferromagnet. Later ARPES studies, optical and quantum oscillation measurements as well as transport data indicated substantial, albeit incomplete, gapping of the Fermi surfaces due to the SDW gap opening.¹³⁻¹⁸ In particular, an optical study by Hu *et al.*¹³ showed the appearance of two gaplike features (GLFs) in the SDW states of BaFe_2As_2 and SrFe_2As_2 , reflecting the multiband nature of the ferropnictides. However, Wu *et al.*¹⁴ reported that the optical conductivity spectra $\sigma(\omega)$ of EuFe_2As_2 showed only one GLF in the SDW state. Hsieh *et al.*,¹⁸ using polarization-dependent ARPES on SrFe_2As_2 , reported two sets of Fermi surfaces, nested and non-nested, and concluded that only the nested bands exhibited a partial gap opening in the SDW state.

The small crystal-field splitting and large bandwidth of the ferropnictide compounds make multiband effects crucial in the formation of the electronic structure both in the vicinity of the Fermi energy and at higher energies.¹⁹⁻²¹ This com-

plicates the interpretation of the electronic structure. Moreover, particularly in AFe_2As_2 compounds, the large magnetic moments cause reconstruction of the electronic bands in the SDW state not only in the vicinity of the Fermi level (as a simplistic nesting picture would imply) but over the entire bandwidth. The multiband and multiorbital nature of the electronic structure suggests an interesting interplay between the orthorhombic anisotropy of the magnetic order (even neglecting the small structural distortion) and the orbital character of the bands near the Fermi level. However, to date, few studies have addressed the effect of magnetism on the multiple electronic bands. In light of this, understanding the changes in the individual electronic bands due to magnetism, and the effects of these changes in spectroscopic quantities such as optical conductivity, is of great interest.

In this paper, we investigate the evolution of the electronic structure of EuFe_2As_2 using optical spectroscopy and density-functional calculations. We observe a drastic decrease in the Drude response and the formation of two GLFs in the $\sigma(\omega)$ across the SDW transition. The GLFs exhibit disparate temperature (T) dependences with one GLF magnitude and spectral weight (SW) in quantitative agreement with the weak-coupling mean-field behavior²² while the other is much less T -dependent. Based on density-functional calculations, we identify the two corresponding classes of optical transitions: one is related to the transition within the spin-minority bands and is therefore sensitive to the long-range magnetic order, and the other between the spin-majority and the spin-minority (on the site with the opposite magnetization) states. The second transition is mostly defined by the local magnetic moment and less sensitive to the long-range ordering.

High-quality EuFe_2As_2 single crystals were grown using the flux technique. Figure 1 shows temperature-dependent in-plane and out-of-plane resistivities (ρ_{ab} and ρ_c) of EuFe_2As_2 single crystal. The resistivities showed a strong

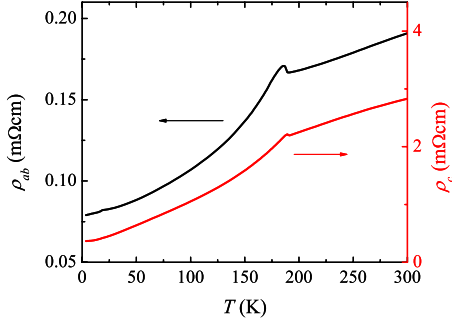


FIG. 1. (Color online) Temperature-dependent in-plane (ρ_{ab}) and out-of-plane (ρ_c) resistivities of EuFe_2As_2 single crystal.

anomaly at $T_{\text{SDW}}=190$ K, which is associated with the SDW transition. The compound remains metallic below T_{SDW} indicating the partial gap opening at the Fermi surface. Another weak kink was observed at about 19 K, which is related to the AFM ordering of the Eu^{2+} spins.^{14,23–25} The difference in ordering temperatures indicates that the energy scale of SDW transition related to Fe ions and AFM ordering of Eu ions are different by an order of magnitude. The magnetic coupling between Fe and Eu ions is negligible as evidenced by the fact that AFM ordering temperature of Eu ions does not depend on SDW transition temperature.²⁶ Near-normal incident reflectance spectra $R(\omega)$ were measured between 5 meV and 6.5 eV, using a liquid-He cooled cryostat. The in-plane $\sigma(\omega)$ were obtained using the Kramers-Kronig transformation of $R(\omega)$. In the calculations, the experimental tetragonal and orthorhombic lattice constants were used for the paramagnetic (PM) and SDW states, respectively.²⁷

Figure 2 displays the T -dependent $\sigma(\omega)$ of EuFe_2As_2 . As T decreases across the SDW transition, the broad Drude-type response becomes strongly suppressed and develops into a gaplike structure. These T -dependent $\sigma(\omega)$ of EuFe_2As_2 reveal a couple of intriguing features. First, in the SDW state, there is a very sharp Drude response in the frequency region below about 0.02 eV. Its small SW and even smaller width, are consistent with a large reduction in the free carrier concentration, due to the opening of a partial gap at the Fermi surface, and an even stronger reduction in the scattering rate, as noticed before.^{28–30} Second, unlike the weight transfer for $\sigma(\omega)$ of single-band density-wave systems, two GLFs (peaks

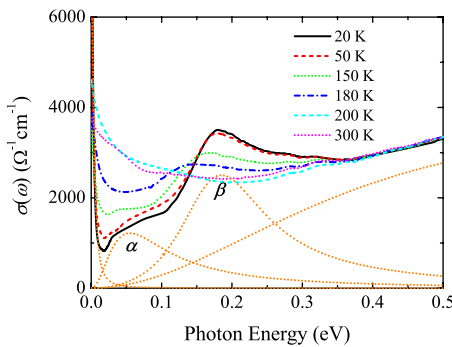


FIG. 2. (Color online) In-plane $\sigma(\omega)$ of EuFe_2As_2 . The dotted lines under the experimental data represent the contributions of the Drude, peak α , peak β , and a high-energy interband optical transition in the Drude-Lorentz oscillator fit at 20 K.

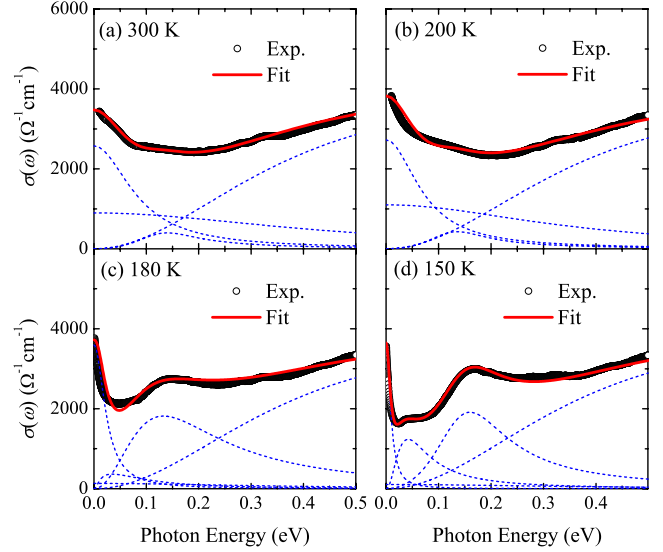


FIG. 3. (Color online) Drude-Lorentz oscillator model fit of $\sigma(\omega)$ at (a) 300 K, (b) 200 K, (c) 180 K, and (d) 150 K.

α and β) appear below the SDW transition that receive the SW lost due to the gapping of the Fermi surface.³¹ The two GLFs was also observed in the $\sigma(\omega)$ of BaFe_2As_2 and SrFe_2As_2 .^{13,32} indicating that this is a generic property of FeAs plane of parent AFe_2As_2 . This clearly reflects the multiband nature of the ferropnictides.

The evolution of these two peaks with T provides insight into the characteristic responses of the individual bands to magnetism. To obtain such information, we analyzed the $\sigma(\omega)$ using the Drude-Lorentz oscillator model.

$$\sigma(\omega) = \sum_i \frac{\omega_{p,i}^2}{4\pi} \frac{\gamma_{Di}}{\omega^2 + \gamma_{Di}^2} + \sum_j \frac{S_j^2}{4\pi} \frac{\gamma_j \omega^2}{(\omega_j^2 - \omega^2)^2 + \gamma_j^2 \omega^2}. \quad (1)$$

The first term describes the coherent response from free carriers while the second term describes the interband transitions. Here, $\omega_{p,i}$ and γ_{D_i} are the plasma frequency and scattering rate of the Drude responses, respectively. ω_j , γ_j , and S_j are the resonance frequency, damping, and strength of each Lorentz oscillator, respectively. The decomposition of $\sigma(\omega)$ at several temperatures is shown in Fig. 3. Overall, we used two Drude (D) terms and three Lorentz oscillators for peak α , peak β , and a high-energy interband transition. The second Drude peak is not necessary for fitting below T_{SDW} , but if we include it, it comes out with a smaller weight and a very large width, and, consequently, with a large uncertainty. According to the Hall data,¹⁷ the hole mobility in the SDW state is drastically smaller than the electron mobility. Thus, we tentatively attribute the first, narrow Drude peak to electrons, and the second, broad and with the SW corresponding to 1.5–2 times smaller Fermi velocity, to holes. Note also that above T_{SDW} the intensity of the low-energy peak α is zero within the fitting uncertainty.

Next we turn to the peak α , which is well-defined below T_{SDW} . We find $2\Delta_\alpha/k_B T_{\text{SDW}} \sim 3.4$, where Δ_α is taken equal to the peak position ω_α at 20 K. Note that this value agrees well with the weak-coupling mean-field BCS ratio. Also, the T dependences of ω_α and SW_α follow the weak-coupling

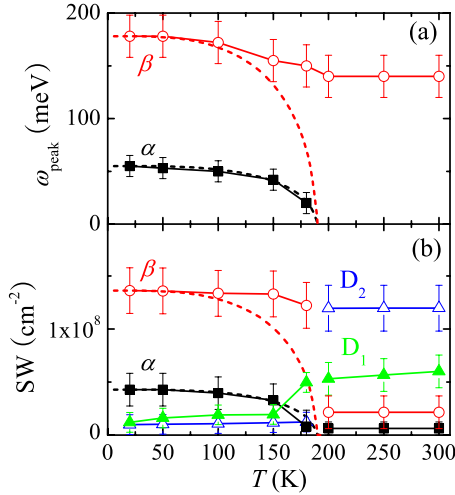


FIG. 4. (Color online) T -dependent changes in (a) the energy values of the peaks α and β and (b) the SW of the peaks α and β , as well as the SW of the two Drude peaks. The dashed lines show the T dependences of the peak energies and SW according to the weak-coupling mean-field BCS theory for the peaks α and β .

mean-field BCS formula quite well, as shown with dashed lines in Figs. 4(a) and 4(b). Conversely, for the peak β , the $2\omega_\beta(20\text{ K})/k_B T_{\text{SDW}}$ value is about 10.9, and there is hardly any T dependence in ω_β and SW_β . Above T_{SDW} , the SW_β abruptly decreases but its position is about the same as that below T_{SDW} . Importantly, the total SW is reasonably well conserved across the transition, with the SW removed from the Drude peaks in the SDW phase, and transferred into the GLF α and β . The overall picture suggests that the peak α is associated with partial gapping that evolves in a mean-field manner while the bands related to the peak β are almost fully gapped and the evolution is a more local phenomenon and involves wholesale alteration of the band structure.

This can be compared with Hsieh *et al.*'s¹⁸ suggestion that two different kinds of bands, nested and non-nested bands, exist in SrFe_2As_2 . They argued that the nested bands experience partial gapping but that the non-nested bands were assumed to have no substantial change upon entering the SDW state. As shown in Fig. 4(b), most of the carriers present above T_{SDW} at the Fermi level E_F disappear below T_{SDW} , and 90% of the Drude SW is shifted into the interband peaks α and β . The discrepancy with the ARPES results most likely is caused by the sensitivity of ARPES (but not optics) to the surface states, which likely have a smaller magnetic moment than in the bulk.

To directly identify the electronic-structure changes in EuFe_2As_2 due to the SDW transition, we performed all-electron density-functional calculations using the local density approximation, as implemented in the WIEN2K code. To avoid complications arising from the f electrons in Eu, our calculations were performed for SrFe_2As_2 with the measured lattice parameters of EuFe_2As_2 . A comparison of the band structures of these two compounds finds that they are virtually identical for 2 eV above and below E_F and the small differences in their electronic structures can be assigned almost exclusively to the change in crystal geometry than to the change in the cation.²³ Moreover, besides the negligible

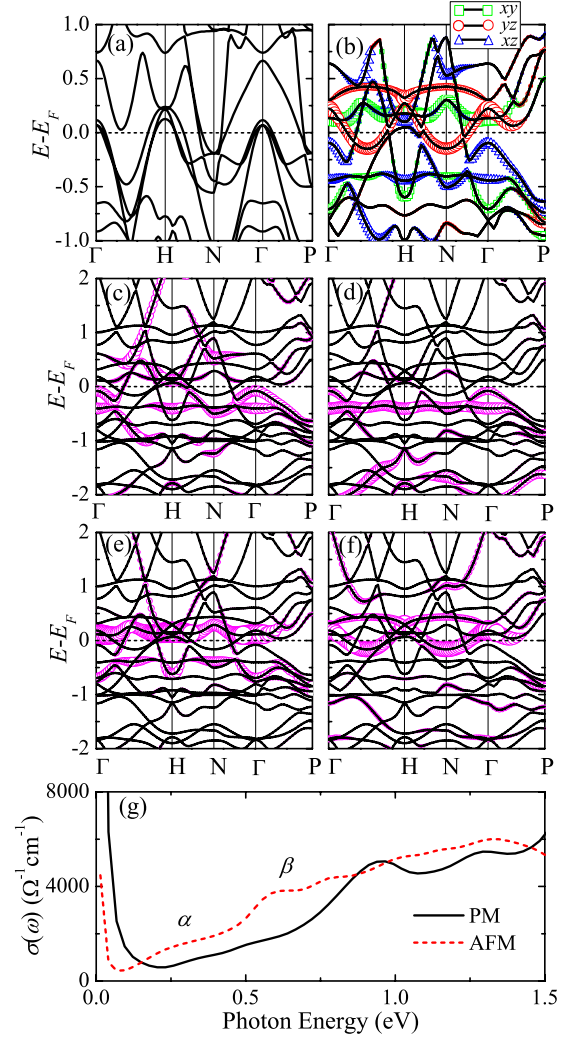


FIG. 5. (Color online) (a) Band structure of the PM tetragonal state. (b) Band structures of the AFM orthorhombic state. The contributions of the xy , yz , and xz orbital states are depicted by the open squares, circles, and triangles. The size of the symbol indicates the fraction of the orbital character of bands. The symmetry points are $\Gamma=(0,0,0)$, $H=(2\pi,0,0)$, $N=(\pi,\pi,0)$, and $P=(\pi/2,\pi/2,\pi/2)$ in the PM Brillouin zone for (a) and AFM Brillouin zone for (b)–(f). Note that the AFM Brillouin zone is rotated by $\pi/4$ relative to that of the tetragonal state and is downfolded. (c) The contribution of Fe-1 d_{xz} spin-up character. (d) The contribution of Fe-1 d_{xz} spin-down character. (e) The Fe-2 d_{xy} spin-down character. Here the Fe-2 atom is adjacent to Fe-1 in the direction of the ordering vector. (f) The Fe-1 d_{yz} spin-up character. (g) Calculated in-plane $\sigma(\omega)$ for the PM and AFM states. As no correlation effects are included in the calculation, the calculated bandwidths are larger by about a factor of 3 compared to the ARPES data (Ref. 34). Therefore, the frequency dependence of the calculated $\sigma(\omega)$ should be scaled down by the same factor in comparing with experimental $\sigma(\omega)$.

magnetic coupling between Fe and Eu ions,^{23–26} the electronic scattering across AFM ordering of Eu ions showed little change while it was drastically reduced across SDW transition.¹⁴ These justify the calculation procedure.

To simulate the actual small experimental magnetic moment of $\sim 1\mu_B$, we applied an artificial negative U of

-0.03 Ry, which reduced the calculated staggered magnetization from $1.65\mu_B$ to $1.15\mu_B$ (this procedure has no physical justification and is only employed to emulate the reduction in the ordered moment due to quantum fluctuations).

Figure 5(a) shows the band structure of the PM state in the energy region between -1 and 1 eV, where the bands have predominantly Fe d character. Near the zone center $\Gamma = (0,0,0)$, three hole bands cross the E_F , while near the $N = (\pi, \pi, 0)$ point, two electron bands cross the E_F . As shown in Fig. 5(b), the band-structure changes drastically upon entering the SDW state. In the SDW state, there are far fewer E_F crossings, and as is evident from Fig. 5(b), these are almost entirely of d_{yz} character.³³ This therefore reflects the gapping of the bands of d_{xy} and d_{xz} character. Here x is the direction of the longer (AFM) Fe-Fe bond and y the direction of the shorter (FM) bond.

Evidently, magnetism affects the band structure on the energy scale of several eV. A comparison of the Fe d_{xz} spin-up and spin-down band character plots in Figs. 5(c) and 5(d) reveals that the spin-up bands of this character lie approximately 1 eV higher than the spin-down bands, and this energy difference carries over to the bands with other orbital characters (not shown) as well. This energy difference can be quantitatively interpreted in terms of exchange splitting, based on the local Fe Hund coupling of ~ 0.8 eV and the calculated staggered magnetization of $1.15\mu_B$. This exchange splitting, not the Hubbard U or Fermi surface nesting, drives the main band-structure changes across the ordering transition.

Moreover, these band-structure changes and Hund coupling can be directly related to the features at about 0.2 and 0.055 eV in the measured $\sigma(\omega)$. Presented in Figs. 5(d) and 5(e) are bands with the Fe d_{xz} spin-down character projection and the d_{xy} projection for the same spin on an antiferromagnetically aligned adjacent Fe, respectively. The latter is identical by symmetry to the spin-up projection on the *same* Fe, therefore they are separated by roughly the exchange splitting.

We immediately notice a flat band in the former projection at approximately -0.4 eV and the latter at 0.2 eV, suggesting the existence of a 0.6 eV feature, which is clearly observed in the calculated $\sigma(\omega)$ [Fig. 5(g)]. This feature results from transitions between the majority occupied Fe spin-down d_{xz} orbital on one Fe atom, Fe-1, and the minority unoccupied spin-down d_{xy} orbital on an adjacent Fe atom with the opposite spin, Fe-2. The parallel nature of the bands then results in a large contribution to the joint density of states (JDOS) at 0.6 eV, which drives the larger gap. (There is of course a similar effect linking the occupied spin-up Fe-2 orbital state with the unoccupied spin-up Fe-1 orbital state.) As this interaction occurs in real space, it is sensitive to the local exchange splitting, and is therefore the harbinger of localized moments. Factoring in the band mass renormalization in the pnictides of approximately 3, as measured through ARPES,³⁴ one concludes that this is the peak β at about 0.2 eV in the measured $\sigma(\omega)$. Supporting this assignment is the fact that this peak is experimentally observed to have little T dependence in the SDW state and to change abruptly its weight (number of instant AFM bonds) but not its position (local moment magnitude) across the magnetic transition.

The origin of the peak α at about 0.055 eV in the measured $\sigma(\omega)$ is somewhat more complex. The d_{yz} spin-up band in Fig. 5(f) is the one that provided metallic carriers at the E_F . In the plot of the d_{xz} spin-up character [Fig. 5(c)] one sees a band parallel to this band but displaced down by approximately 0.25 eV. These parallel bands provide a distinct contribution to JDOS and result in a feature at 0.25 eV in the calculated $\sigma(\omega)$. Unlike the larger gap, however, this gap originates from transitions between two same-spin orbitals within the *same-spin* sublattice, and is therefore insensitive to the local exchange splitting (we have verified that reducing the local moment in the calculations moves the associated 0.4 and -0.2 eV bands closer but affects little the lower-energy feature). This gap is thus an itinerant-type SDW one, despite substantial band-structure effects. Considering the mass renormalization factor, we conclude that this smaller peak is the peak α seen at 0.055 eV in the experiment, which obeys markedly mean-field BCS-type behavior.

The magnetism in the ferropnictides is thus neither fully local nor fully itinerant, but has elements of both, as discussed in Ref. 35. In recent inelastic neutron-scattering study on CaFe_2As_2 , Zhao *et al.*³⁶ showed that the spin waves throughout the Brillouin zone could be fit with a simple Heisenberg Hamiltonian. While this result favors a local moment picture, a possible importance of itinerant character of magnetism was suggested due to the in-plane anisotropy of exchange interaction. Qazilbash *et al.*³⁷ reported that ferropnictides are classified as being in a moderate correlation regime and argued that they lie between the bandlike itinerant and the Mott-type local magnetic moments extremes.

Our experiment shows that this duality translates into two distinctively different sets of optical features. One is a low-energy feature that monitors the true long-range order manifesting itself in restructuring the Fermi surface and thereby gapping out the Drude SW. This spatial ordering is comparable to the conventional spin-Peierls SDW, except it develops on the background of the large local moments, which produce substantial band-structure changes. The higher-energy feature is less sensitive to the long-range spatial order but rather to the local exchange splitting. Intermediate-range ordering is sufficient to slow down the local fluctuations enough to make the local splitting visible in optics.

In summary, we have investigated the electronic structure of EuFe_2As_2 using optical spectroscopy and density-functional calculations. We observe drastic changes in the optical conductivity across the spin-density-wave transition, which can be described as transfer of the spectral weight into two gaplike features. These are very sensitive to the symmetry breaking associated with the stripe antiferromagnetism. The higher-energy feature is associated with the optical transitions between two Fe atoms of the opposite spin. The scale is set by the local exchange splitting, therefore this transition shows little temperature dependence below T_{SDW} and survives (with a reduced spectral weight) above T_{SDW} . The low-energy feature is associated with the transitions within the spin-minority states of the same-spin Fe's. These are less sensitive to the magnitude of exchange splitting but very sensitive to the long-range order controlling the gapping of the Fermi surface. Thermally this feature behaves as a weak-coupling spin-density-wave order parameter. We conclude

that magnetic ordering in pnictides is a complex two-level process with some states behaving as local and others as itinerant, and the models using only one side of this combination are necessarily incomplete. This applies to both theoretical constructions and interpretations of spectroscopic experiments.

We acknowledge valuable discussions with S. Y. Park and H. J. Choi. This research was supported by Basic Science Research Program through the National Research Founda-

tion of Korea funded by the Ministry of Education, Science and Technology (MEST) (Grant No. 2009-0080567). Y.S.L. was supported by Basic Science Research Program through the National Research Foundation of Korea funded by the MEST (Grant No. 2009-0076978). The work at GIST was supported by the Korean Science and Engineering Foundation funded by MEST (Grant No. 2009-0078928). K.H.K. is supported by the NRL program (Grant No. M10600000238) by MEST.

*davidspa@dave.nrl.navy.mil

†twnoh@snu.ac.kr

- ¹Y. Kamihara, T. Watanabe, M. Hirano, and H. Hosono, *J. Am. Chem. Soc.* **130**, 3296 (2008).
- ²C. de la Cruz, Q. Huang, J. W. Lynn, J. Li, W. Ratcliff II, J. L. Zarestky, H. A. Mook, G. F. Chen, J. L. Luo, N. L. Wang, and P. Dai, *Nature (London)* **453**, 899 (2008).
- ³M. Rotter, M. Tegel, D. Johrendt, I. Schellenberg, W. Hermes, and R. Pöttgen, *Phys. Rev. B* **78**, 020503(R) (2008).
- ⁴J. Zhao, W. Ratcliff, J. W. Lynn, G. F. Chen, J. L. Luo, N. L. Wang, J. Hu, and P. Dai, *Phys. Rev. B* **78**, 140504(R) (2008).
- ⁵Q. Huang, Y. Qiu, W. Bao, M. A. Green, J. W. Lynn, Y. C. Gasparovic, T. Wu, G. Wu, and X. H. Chen, *Phys. Rev. Lett.* **101**, 257003 (2008).
- ⁶X. H. Chen, T. Wu, G. Wu, R. H. Liu, H. Chen, and D. F. Fang, *Nature (London)* **453**, 761 (2008).
- ⁷M. Rotter, M. Tegel, and D. Johrendt, *Phys. Rev. Lett.* **101**, 107006 (2008).
- ⁸M. S. Torikachvili, S. L. Bud'ko, N. Ni, and P. C. Canfield, *Phys. Rev. Lett.* **101**, 057006 (2008).
- ⁹H. Takahashi, K. Igawa, K. Arii, Y. Kamihara, M. Hirano, and H. Hosono, *Nature (London)* **453**, 376 (2008).
- ¹⁰I. I. Mazin and J. Schmalian, *Physica C* **469**, 614 (2009).
- ¹¹L. X. Yang, Y. Zhang, H. W. Ou, J. F. Zhao, D. W. Shen, B. Zhou, J. Wei, F. Chen, M. Xu, C. He, Y. Chen, Z. D. Wang, X. F. Wang, T. Wu, G. Wu, X. H. Chen, M. Arita, K. Shimada, M. Taniguchi, Z. Y. Lu, T. Xiang, and D. L. Feng, *Phys. Rev. Lett.* **102**, 107002 (2009).
- ¹²Y. Zhang, J. Wei, H. W. Ou, J. F. Zhao, B. Zhou, F. Chen, M. Xu, C. He, G. Wu, H. Chen, M. Arita, K. Shimada, H. Namatame, M. Taniguchi, X. H. Chen, and D. L. Feng, *Phys. Rev. Lett.* **102**, 127003 (2009).
- ¹³W. Z. Hu, J. Dong, G. Li, Z. Li, P. Zheng, G. F. Chen, J. L. Luo, and N. L. Wang, *Phys. Rev. Lett.* **101**, 257005 (2008).
- ¹⁴D. Wu, N. Barišić, N. Driehko, S. Kaiser, A. Faridian, M. Dressel, S. Jiang, Z. Ren, L. J. Li, G. H. Cao, Z. A. Xu, H. S. Jeevan, and P. Gegenwart, *Phys. Rev. B* **79**, 155103 (2009).
- ¹⁵F. Pfuner, J. G. Analytis, J.-H. Chu, I. R. Fisher, and L. De-giorgi, *Eur. Phys. J. B* **67**, 513 (2009).
- ¹⁶S. E. Sebastian, J. Gillett, N. Harrison, P. H. C. Lau, D. J. Singh, C. H. Mielke, and G. G. Lonzarich, *J. Phys.: Condens. Matter* **20**, 422203 (2008).
- ¹⁷L. Fang, H. Luo, P. Cheng, Z. Wang, Y. Jia, G. Mu, B. Shen, I. I. Mazin, L. Shan, C. Ren, and H.-H. Wen, *Phys. Rev. B* **80**, 140508(R) (2009); F. Rullier-Albenque, D. Colson, A. Forget, and H. Alloul, *Phys. Rev. Lett.* **103**, 057001 (2009).
- ¹⁸D. Hsieh, Y. Xia, L. Wray, D. Qian, K. Gomes, A. Yazdani, G. Chen, J. Luo, N. Wang, and M. Hasan, [arXiv:0812.2289](https://arxiv.org/abs/0812.2289) (unpublished).
- ¹⁹D. J. Singh, *Phys. Rev. B* **78**, 094511 (2008).
- ²⁰F. Ma, Z.-Y. Lu, and T. Xiang, *Phys. Rev. B* **78**, 224517 (2008).
- ²¹I. I. Mazin, D. J. Singh, M. D. Johannes, and M. H. Du, *Phys. Rev. Lett.* **101**, 057003 (2008).
- ²²G. Grüner, *Density Waves in Solids* (Addison-Wesley, Los Angeles, 1994).
- ²³H. S. Jeevan, Z. Hossain, D. Kasinathan, H. Rosner, C. Geibel, and P. Gegenwart, *Phys. Rev. B* **78**, 052502 (2008).
- ²⁴C. F. Miclea, M. Nicklas, H. S. Jeevan, D. Kasinathan, Z. Hossain, H. Rosner, P. Gegenwart, C. Geibel, and F. Steglich, *Phys. Rev. B* **79**, 212509 (2009).
- ²⁵S. Jiang, Y. Luo, Z. Ren, Z. Zhu, C. Wang, X. Xu, Q. Tao, G. Cao, and Z. Xu, *New J. Phys.* **11**, 025007 (2009).
- ²⁶Q. Zheng, Y. He, T. Wu, G. Wu, H. Chen, J. Ying, R. Liu, X. Wang, Y. Xie, Y. Yan, Q. Li, and X. Chen, [arXiv:0907.5547](https://arxiv.org/abs/0907.5547) (unpublished).
- ²⁷M. Tegel, M. Rotter, V. Weiß, F. M. Schappacher, R. Pöttgen, and D. Johrendt, *J. Phys.: Condens. Matter* **20**, 452201 (2008).
- ²⁸W. Z. Hu, Q. M. Zhang, and N. L. Wang, *Physica C* **469**, 545 (2009).
- ²⁹Z. G. Chen, G. Xu, W. Z. Hu, X. D. Zhang, P. Zheng, G. F. Chen, J. L. Luo, Z. Fang, and N. L. Wang, *Phys. Rev. B* **80**, 094506 (2009).
- ³⁰J. S. Lee, S. J. Moon, B. J. Yang, J. Yu, U. Schade, Y. Yoshida, S.-I. Ikeda, and T. W. Noh, *Phys. Rev. Lett.* **98**, 097403 (2007).
- ³¹In Ref. 14, the low-energy gaplike feature was observed in the extended Drude model analysis as well as $\sigma(\omega)$ itself. Instead of assigning the low-energy gaplike feature, it was proposed that a broad electronic background, Drude response, might exist at all temperatures.
- ³²A. Akrap, J. J. Tu, L. J. Li, G. H. Cao, Z. A. Xu, and C. C. Homes, *Phys. Rev. B* **80**, 180502(R) (2009).
- ³³T. Shimojima, K. Ishizaka, Y. Ishida, N. Katayama, K. Ohgushi, T. Kiss, M. Okawa, T. Togashi, X.-Y. Wang, C.-T. Chen, S. Watanabe, R. Kadota, T. Oguchi, A. Chainani, and S. Shin, *Phys. Rev. Lett.* **104**, 057002 (2010).
- ³⁴D. H. Lu, M. Yi, S.-K. Mo, A. S. Erickson, J. Analytis, J.-H. Chu, D. J. Singh, Z. Hussain, T. H. Geballe, I. R. Fisher, and Z.-X. Shen, *Nature (London)* **455**, 81 (2008).
- ³⁵M. D. Johannes and I. I. Mazin, *Phys. Rev. B* **79**, 220510(R) (2009).
- ³⁶J. Zhao, D. T. Adroja, D.-X. Yao, R. Bewley, S. Li, X. F. Wang, G. Wu, X. H. Chen, J. Hu, and P. Dai, *Nat. Phys.* **5**, 555 (2009).
- ³⁷M. M. Qazilbash, J. J. Hamlin, R. E. Baumbach, L. Zhang, D. J. Singh, M. B. Maple, and D. N. Basov, *Nat. Phys.* **5**, 647 (2009).